iScience

CellPress
OPEN ACCESS

Article

Gut commensal *Agathobacter rectalis* alleviates microglia-mediated neuroinflammation against pathogenesis of Alzheimer disease

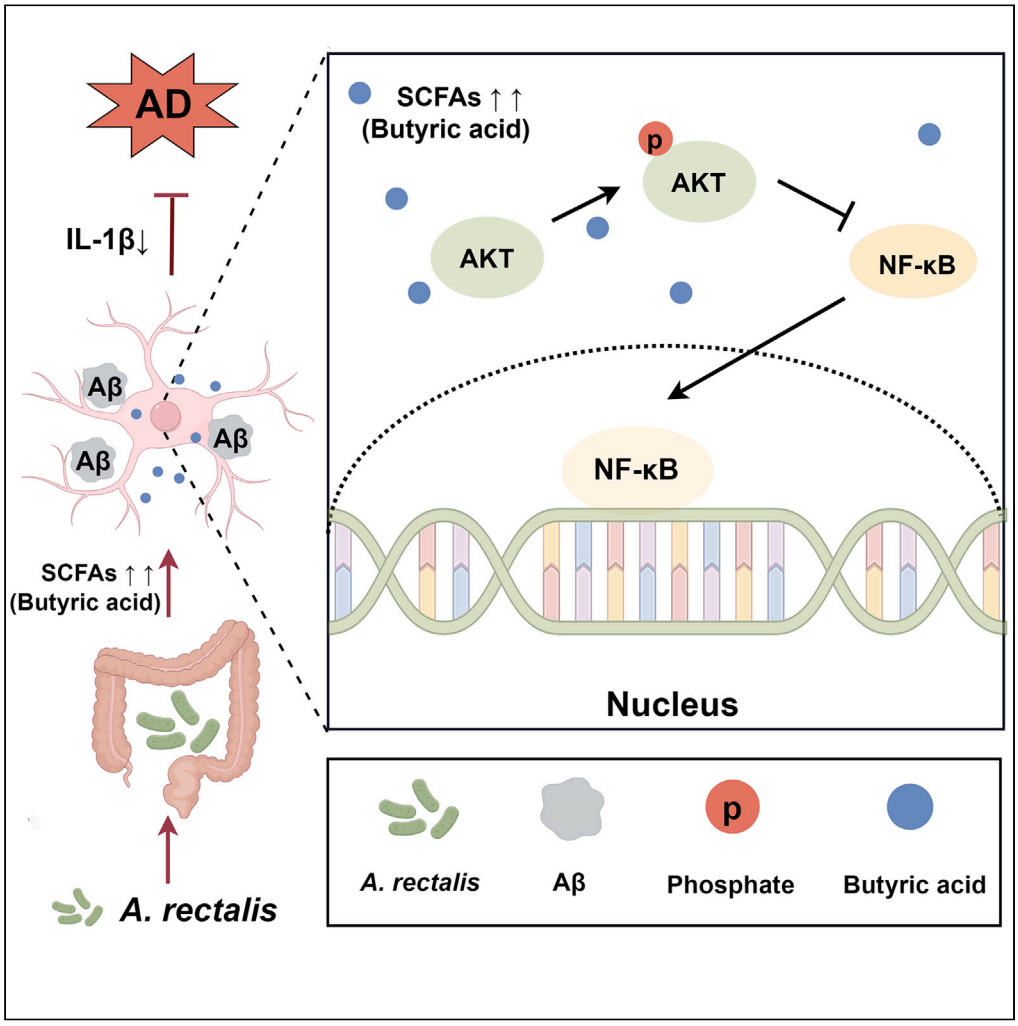

Xinhuang Lv, Lu Zhan, Tao Ye, ..., Xiaolan Liao, Jiaming Liu, Jing Sun

wzjiaming_liu@163.com (J.L.)
sunjwz@126.com (J.S.)

Highlights

Agathobacter deficiency in AD patients was associated with cognitive impairment

A. rectalis treatment improved cognitive impairment and neuroinflammation in AD mice

A. rectalis-derived butyrate inhibited microglia activation via Akt/NF-κB pathway

The findings provide insights into the correlation between specific bacteria and AD

Lv et al., iScience 27, 111116
November 15, 2024
https://doi.org/10.1016/j.isci.2024.111116

iScience

CellPress
OPEN ACCESS

Article

Gut commensal *Agathobacter rectalis* alleviates microglia-mediated neuroinflammation against pathogenesis of Alzheimer disease

Xinhuang Lv,[1,4] Lu Zhan,[2,4] Tao Ye,[1,4] Huijia Xie,[1,4] Zhibo Chen,[3] Yan Lin,[1] Xianlei Cai,[2] Wenwen Yang,[2] Xiaolan Liao,[1] Jiaming Liu,[2,5,*] and Jing Sun[1,*]

SUMMARY

Gut microbiota plays a crucial role in the pathogenesis of Alzheimer disease (AD). Here, we found that AD patients had significantly lower abundance of *Agathobacter*, which were negatively correlated with cognitive impairment. Animal experiments showed that *Agathobacter rectalis (A. rectalis)* supplementation increased beneficial commensal bacteria, significantly improved pathological damage, and suppressed microglial activation in APP/PS1 mice. We further demonstrated that butyric acid, a metabolite of *A. rectalis*, reduced microglial activation and pro-inflammatory factor production via Akt/ nuclear factor κB (NF-κB) signal pathway *in vitro*. Meanwhile, we revealed that *A. rectalis* effectively inhibited activation of microglia in the APP/PS1 mice by regulating Akt/ NF-κB pathway. This finding highlights the role of *A. rectalis* and its metabolite butyrate in mitigating neuroinflammation in AD by modulating the Akt/NF-κB pathway.

INTRODUCTION

Alzheimer disease (AD) is a progressive neurodegenerative disease associated with genetic mutations, epigenetic changes, and gut microbiota dysbiosis.[1,2] An increasing number of studies have shown changes in the gut microbiota composition of AD patients. These abnormal gut bacteria are closely related to the development and progression of AD. The potential mechanisms may include the regulation of amyloid β-protein, tau phosphorylation, and microglia activation.[3–5] Recent research has increasingly focused on the role of gut microbiota in the neuroinflammation of AD, particularly in microglia activation.[6,7] The changes in the gut microbiota alter the transcriptome and affect microglia maturation and polarization.[8,9] Our previous study showed that healthy fecal microbiota transplantation could be employed to decrease the levels of M1 microglial polarization markers COX-2 and CD11b and inhibit microglia-mediated neuroinflammation in the APP/PS1 mice.[6] Gut microbiota could elicit distinct signaling to the brain and exerted regulatory effects on microglia. However, the exact mechanisms by which gut microbiota induce microglia activation in AD remain unknown.

The microbiota-gut-brain axis bidirectionally transmits information between gut and brain.[10] Various preclinical and clinical studies have supported the notion that disturbances in the composition of gut microbiota play an important role in the neuroinflammation of AD. Recently, increasing evidence has demonstrated that some beneficial bacteria could inhibit microglia activation and decrease neuroinflammation, potentially contributing to AD prevention.[11,12] Nevertheless, the specific mechanisms of this communication and its putative effects on the neuroinflammation and cognitive function are largely unknown. Emerging evidence has shown that metabolites derived from gut microbiota were critical in microbiota-gut-brain crosstalk.[7,13,14] Moreover, the exacerbation or improvement of neuroinflammation is linked to different gut microbiota and metabolites, and further investigation is warranted to comprehend the intricate relationship between them. Our previous study has shown that probiotic *Clostridium butyricum* significantly regulated abnormal gut microbiota and reduced neuroinflammatory response, possibly due to the suppression of microglia activation through production of short-chain fatty acid (SCFA) butyric acid.[15] Recent studies have highlighted that SCFAs, the primary metabolites from gut bacterial fermentation, specifically modulate microglial activation.[14,16] The dysbiosis in AD mice can be transferred to healthy mice through co-cage feeding or fecal microbiota transplantation, leading to gut dysbiosis, and reduce the content of butyric acid in the brain, further triggering cognitive impairment.[17] Despite there is substantial evidence linking AD to gut microbiota, few studies have examined the association with specific commensal bacteria and neuroinflammation. Therefore, it is necessary to identify and apply certain commensal bacteria that directly and specifically affect the microglia activation of AD, thereby enhancing the anti-neuroinflammation and improving cognitive function.

[1]Department of Geriatrics, the Second Affiliated Hospital and Yuying Children's Hospital of Wenzhou Medical University, Wenzhou 325027, Zhejiang, China
[2]Department of Preventive Medicine, School of Public Health, Wenzhou Medical University, Wenzhou 325027, Zhejiang, China
[3]Department of Neurology, the First Affiliated Hospital of Wenzhou Medical University, Wenzhou 325027, Zhejiang, China
[4]These authors contributed equally
[5]Lead contact
*Correspondence: wzjiaming_liu@163.com (J.L.), sunjwz@126.com (J.S.)
https://doi.org/10.1016/j.isci.2024.111116

In this study, we observed that the abundance of *Agathobacter* was reduced in AD patients, and the abundance of *Agathobacter* was negatively correlated with cognitive impairment. We confirmed the effect of commensal bacteria *Agathobacter* on the microglial activation of AD in the APP/PS1 mice and further demonstrated that butyric acid, a metabolite of *Agathobacter rectalis*, suppressed microglial activation to improve neuroinflammation of AD via regulating Akt/nuclear factor κB (NF-κB) signal pathway *in vitro*. Meanwhile, we revealed that *A. rectalis* effectively inhibited activation of microglia in the APP/PS1 mice by regulating Akt/NF-κB pathway. Our research comprehensively explored how specific bacterial and its metabolite butyric acid influence neuroinflammation and AD progression. Thus, we clearly showed a causal relationship between specific bacterial members from gut microbiota and neuroinflammation of AD.

RESULTS

Gut commensal *Agathobacter* was reduced in AD patients and negatively correlated with cognitive impairment

To investigate the relationship between gut microbiota and AD, we first performed 16s rRNA sequencing of fecal samples in AD patients and healthy controls (HCs). Alpha diversity, as measured by Shannon and Simpson indices, showed no significant difference between the AD group and HC group (Figures 1A and 1B). Principal coordinate analysis (PCoA) also revealed no significant difference in gut microbiota between the HC and AD groups (Figure 1C). Regarding the genus differences, the AD group had lower *Escherichia-Shigella*, *Faecalibacterium*, *Ruminococcus*, and *Agathobacter* than the HC group (Figure 1D). Based on linear discriminant analysis effect size (LEfSe) method, we found that the HC group was characterized by enriched *Agathobacter*, *Monoglobus*, *Dorea*, *Fusobacterium*, *Butyricicoccus*, *Lachnospira*, and *Rothia*, whereas unclassified_c_Bacilli, *Bacillus*, norank_f_Erysipelotrichaceae, and *Christensenea* were dominant bacteria in the AD group (Figure 1E). Heatmap of spearman correlation suggested the relative abundance of *Agathobacter* was significantly negatively correlated with MMSE and MOCA scores ($p < 0.01$, Figure 1E). Furthermore, we determined the abundance of *Agathobacter* and observed that *Agathobacter* were significantly lower in the AD group compared to the HC group ($p < 0.05$, Figure 1F). Given that known *Agathobacter* is a producer of SCFAs, we performed GC-MS of fecal samples in AD patients to elevate SCFAs changes in AD. We observed a significant reduction in butyric acid level in the AD group compared to the HC group ($p < 0.05$, Figure 1G). A linear regression analysis showed a positive association between the abundance of *Agathobacter* and SCFA butyric acid level ($p < 0.05$, Figure 1H). The aforementioned results suggested that *Agathobacter* has the potential to serve as a bacterium that indicate the benefits of AD phenotypes.

A. rectalis supplementation improved cognitive impairment and pathological changes in the APP/PS1 mice

To investigate the beneficial effect of *Agathobacter* in cognitive function of AD, we conducted a battery of behavioral tests, including the nesting test, object recognition test, and Barnes maze test. In the nesting test, the nesting score in PBS-treated group was significantly decreased compared to the WT group, whereas the score in *A. rectalis*-treated mice was markedly increased than the PBS-treated mice ($p < 0.05$, Figure 2A). In the object recognition test, the discriminant index was significantly decreased in PBS-treated mice compared with wild-type (WT) group, whereas it was restored by *A. rectalis* treatment ($p < 0.05$, Figure 2B). In addition, the latency for the mice to find the target box gradually shortened on days 1 and 2 as the experiment progressed. On days 3 and 4, the latency of *A. rectalis*-treated mice was significantly shortened than the PBS-treated mice ($p < 0.05$, Figure 2C). The time spent in the target quadrant in the *A. rectalis*-treated mice was significantly increased compared to that of PBS-treated mice ($p < 0.05$, Figure 2D). These results indicated that *A. rectalis* could attenuate cognitive impairment.

To evaluate the effects of *A. rectalis* on pathological changes in AD, Nissl staining, Aβ deposit, and tau phosphorylation detection were conducted. As shown in Figure 2E, the expression level of $A\beta_{42}$ in the *A. rectalis*-treated mice was decreased compared to that in the PBS-treated mice ($p < 0.05$, Figure 2F). Then, we further evaluated the level of $A\beta_{42}$ by western blot. The level of $A\beta_{42}$ in the *A. rectalis*-treated mice was markedly decreased compared to that in the PBS-treated mice ($p < 0.01$, Figures 2G and 2H). As shown in Figure 3A, in Nissl staining, the number of Nissl bodies was reduced in the PBS-treated group, whereas the neurons were in order, and there were more numerous Nissl bodies in the *A. rectalis*-treated group. The level of tau phosphorylation in the *A. rectalis*-treated mice was decreased markedly compared with that in the PBS-treated mice ($p < 0.01$, Figures 3B–3D). These results indicated that *A. rectalis* treatment could alleviate AD-like pathology in the APP/PS1 mice.

A. rectalis treatment suppressed microglia-mediated neuroinflammation in the APP/PS1 mice

To investigate the effect of *A. rectalis* on the activation of microglia in AD, the levels of Iba1 was assessed by immunohistochemistry. As shown in Figure 4A, the expression level of Iba1 in the *A. rectalis*-treated mice was decreased than that in the PBS-treated mice. PCR analysis of microglial subtypes in mice revealed that *A. rectalis* treatment did not significantly affect the markers of homeostatic microglia (Figure S1A), proliferating microglia (Figure S1B), or interferon-response microglia (Figure S1D). However, it significantly decreased the expression of the disease-associated microglia marker CD33 ($p < 0.05$, Figures S1C and S1F) and the aged microglia markers tumor necrosis factor alpha (TNF-α) and interleukin-1β (IL-1β) ($p < 0.05$, Figures S1E and S1F). Immunofluorescence staining of Aβ and Iba1 showed that *A. rectalis* treatment improved their morphology such as cell size and branching levels compared to the PBS group (Figure 4B). Meanwhile, in western blot, the levels of Iba1, CD11b, and iNOS in the *A. rectalis*-treated mice was significantly decreased compared to that in PBS-treated mice (Iba1: $p < 0.01$, CD11b: $p < 0.01$, iNOS: $p < 0.05$, Figures 4C and 4D). Subsequently, we observed TREM2 was significantly increased in the *A. rectalis*-treated mice compared to that in the PBS-treated mice ($p < 0.05$, Figures 4C and 4D). However, the level of TMEM119 was unchanged in *A. rectalis*-treated mice compared to PBS group (Figures 4C and 4D).

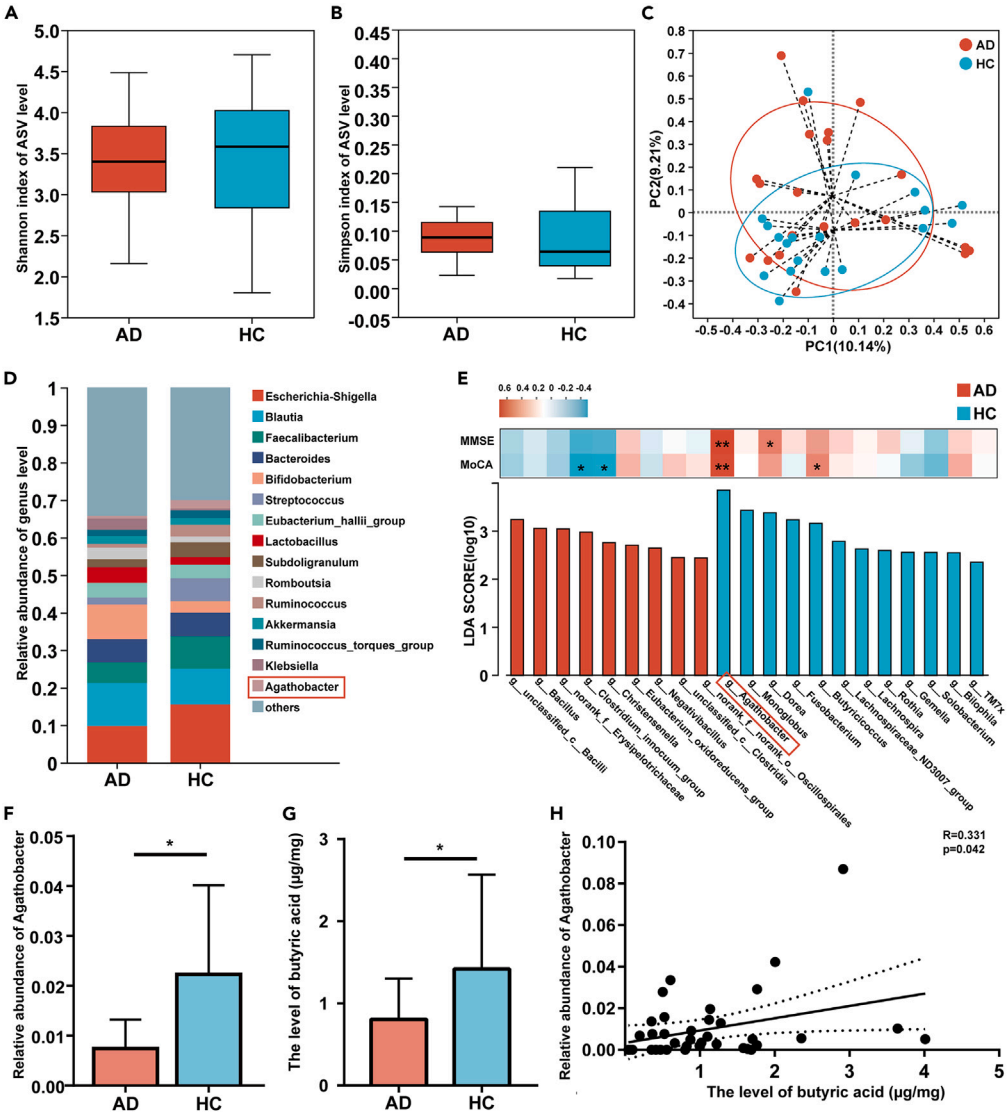

Figure 1. Gut commensal *Agathobacter* was reduced in AD patients and negatively correlated with cognitive impairment

(A) Shannon index of gut microbiota α-diversity in AD patients and healthy controls (HCs).

(B) Simpson index of gut microbiota α-diversity in AD patients and HCs.

(C) PCoA with Bray-Curtis distances showing differences between AD patients and HC bacterial community.

(D) Stacked bar chart displaying the community structure composition and relative abundance of genus level in AD patients and HCs.

(E) LEfSe analysis showing significant bacterial differences between AD patients (red) and HCs (blue). LDA >2 and $p < 0.05$ were listed. Furthermore, heatmap based on spearman correlation analysis showing the correlation between differential bacteria and clinical indicators, such as MMSE and MOCA scores.

(F) Comparisons of the abundance of *Agathobacter* between AD patients and HCs.

(G) Comparisons of butyric acid level between AD patients and HCs.

(H) The linear regression analysis based on spearman correlation between *Agathobacter* and butyric acid level. Data are shown as medians and interquartile ranges (A and B) or mean ± SEM (F and G). *p values* were determined by Mann-Whitney test (A, B, and F) or Welch's t test (G). *$p < 0.05$ vs. AD group, **$p < 0.01$ vs. AD group.

Butyric acid treatment suppressed microglia-mediated neuroinflammation in LPS-induced BV2 microglia cells via modulating Akt/NF-κB pathway

To further clarify the potential anti-inflammatory mechanisms of *A. rectalis*, we analyzed the effect of *A. rectalis* metabolite butyric acid on microglia activation *in vitro*. In lipopolysaccharide (LPS)-induced BV2 cells model, the expression level of COX-2 in the LPS + NaB group was decreased compared with that in the LPS group ($p < 0.01$, Figures 5A and 5C). As shown in Figures 5B and 5D, the expression level of ROS in the LPS + NaB group was decreased significantly compared with that in the LPS group ($p < 0.01$). Western blot analyses revealed

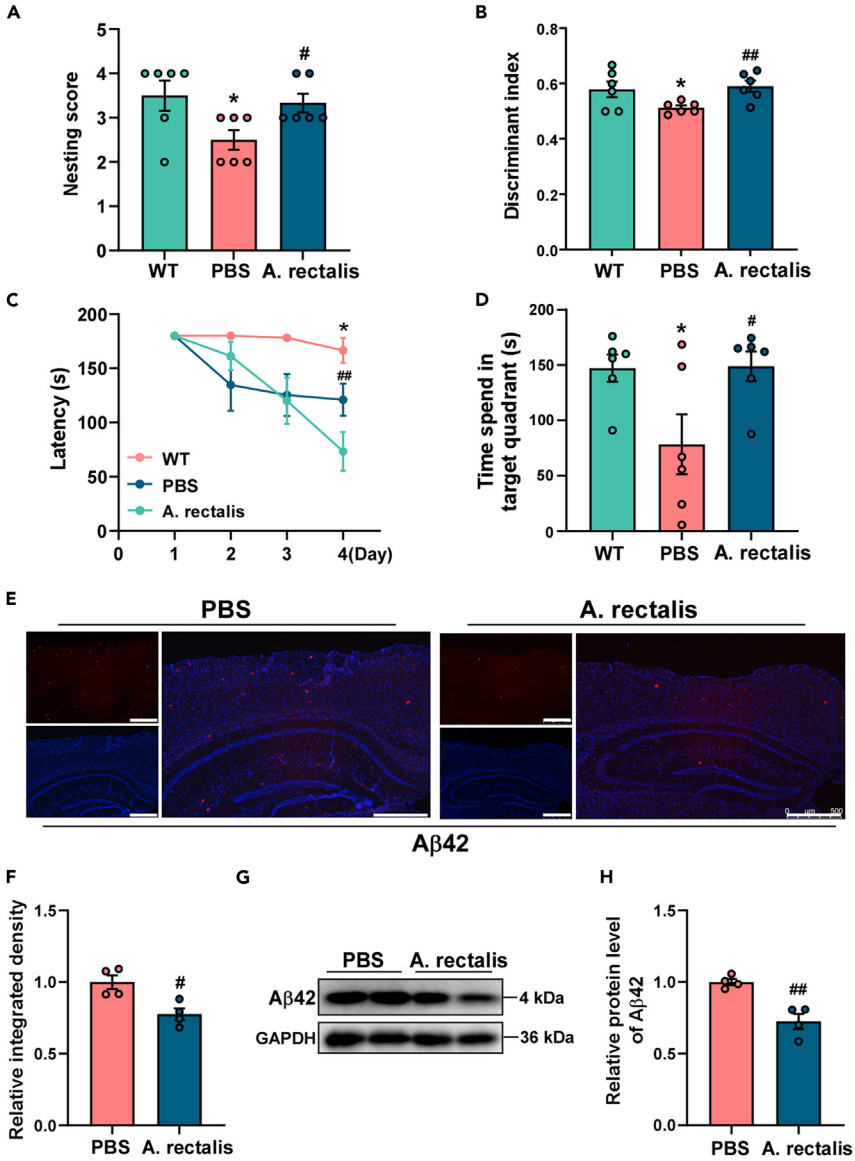

Figure 2. *A. rectalis* supplementation improved cognitive impairment and decreased Aβ level in the APP/PS1 mice

(A) Comparisons of Nesting score among the WT group, PBS-treated group, and *A. rectalis*-treated group.

(B) Comparisons of discriminant index among three groups.

(C) Comparisons of latency in Barnes maze test among three groups.

(D) Time spent in target quadrant in Barnes maze test.

(E) Representative immunofluorescence images of $A\beta_{42}$ in the brain. Magnification 50×; scale bar, 500 μm.

(F) Quantitative analysis of $A\beta_{42}$ level.

(G) Representative western blot images of $A\beta_{42}$.

(H) Quantitative analysis of $A\beta_{42}$ expression. The ratio of $A\beta_{42}$/GAPDH in the PBS-treated group was used as the reference value. Data are shown as mean ± SEM. *p* values were determined by one-way ANOWA (A, B, and D) or two-way ANOWA (C) or unpaired two-tailed t test (F and H). $^{*}p < 0.05$ vs. WT group; $^{\#}p < 0.05$ vs. PBS-treated group; $^{\#\#}p < 0.01$ vs. PBS-treated group.

that the levels of iNOS and IL-1β in the LPS + NaB group were significantly decreased compared to that in the LPS group (iNOS: $p < 0.01$, IL-1β: $p < 0.01$, Figures 5E and 5F). In addition, in Aβ-induced BV2 cells model, the level of COX-2 in the NaB-treated group was also significantly decreased, compared to that in the Aβ-induced group ($p < 0.001$, Figures S2A and S2B), and the levels of iNOS and IL-1β in the NaB-treated group was significantly decreased compared to that in the Aβ-induced group (iNOS: $p < 0.05$, IL-1β: $p < 0.01$, Figures S2C and S2D). These data suggested that butyric acid could inhibit M1 microglial polarization.

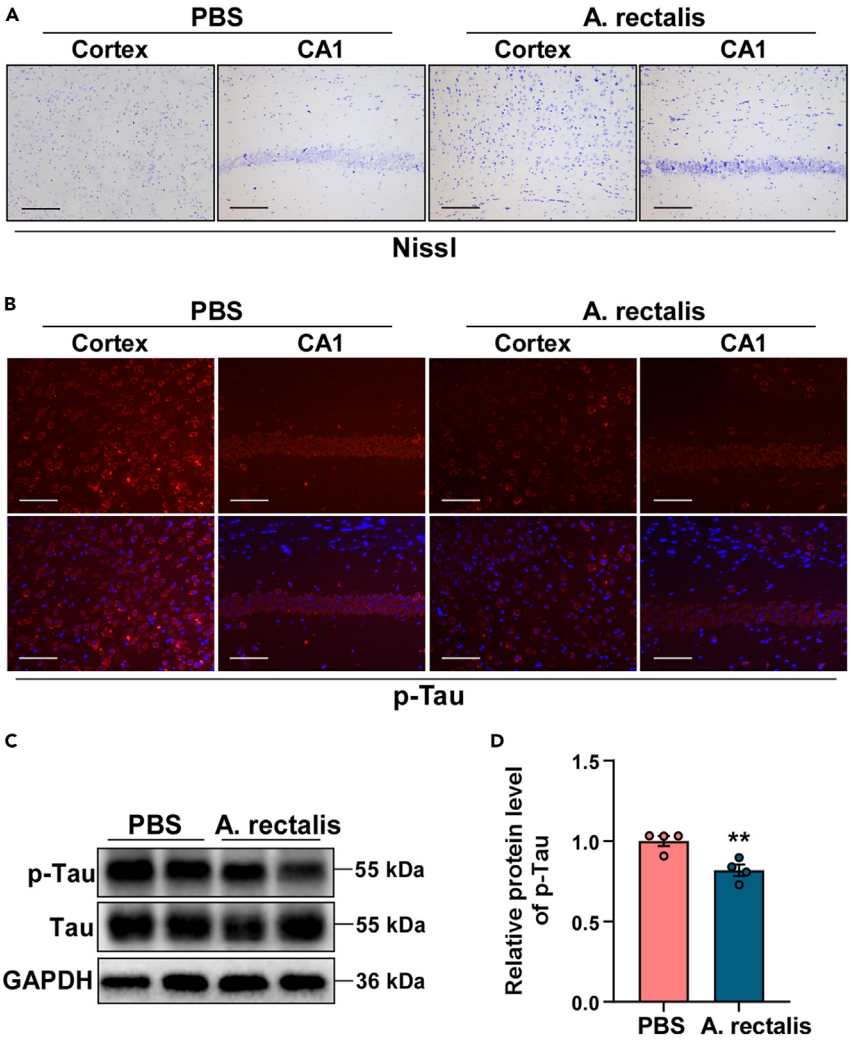

Figure 3. *A. rectalis* supplementation improved pathological changes in the APP/PS1 mice

(A) Representative Nissl staining images. Magnification 200×; scale bar, 100 μm.

(B) Representative immunofluorescence images of p-Tau. Magnification 200×; scale bar, 100 μm.

(C) Representative western blot images of p-Tau and Tau.

(D) Quantitative analysis of p-Tau expression. The ratio of p-Tau/Tau in the PBS-treated group was used as the reference value. Data are shown as mean ± SEM. *p* values were determined by unpaired two-tailed t test (D). $^{**}p < 0.01$ vs. PBS-treated group.

To clarify the molecular mechanism of butyric acid on the suppression of microglia activation, we performed RNA sequencing (RNA-seq) analysis to identify differentially expressed genes (DEGs) in the LPS-induced BV2 microglia with or without NaB treatment ($|\log2FC| > 1.2$, $p < 0.05$). Volcano plot showed the distribution of DEGs between two groups (Figure 6A). Heatmap visually displayed the top 20 DEGs between two groups (Figure 6B). To further probe the potential impact of NaB treatment on LPS-induced BV2 microglia, we performed Gene Ontology (GO) term and KEGG pathway enrichment analyses on the DEGs identified from the sequencing results. The GO Biological Process analysis indicated that NaB treatment mainly affected the biological functions of immunity and inflammation in the LPS-induced BV2 cells (Figure 6C). Then, KEGG analysis revealed significant differences in the Akt and NF-κB signaling pathways on the DEGs (Figure 6D). Combined with the results of GO analysis, we hypothesize that NaB may regulate the Akt pathway and its downstream pathway NF-κB to participate in the inflammatory process of BV2 microglia cells. To confirm our hypothesize, Akt- and NF-κB-pathway-related proteins detection were conducted. Western blot analysis revealed that the ratio of p-Akt/Akt in LPS + NaB group was markedly higher than that in the LPS group ($p < 0.05$, Figures 6E and 6F), whereas the ratio of p-p65/p65 in LPS + NaB group was significantly lower than that in the LPS group ($p < 0.01$, Figures 6E and 6F). Those results were also observed in Aβ-induced BV2 cells. Western blot analysis revealed that the ratio of p-Akt/Akt in Aβ + NaB group was markedly higher than that in the Aβ-induced group ($p < 0.01$, Figures S2E and S2F). Moreover, the ratio of p-p65/p65 in Aβ + NaB group was significantly lower than that in the Aβ-induced

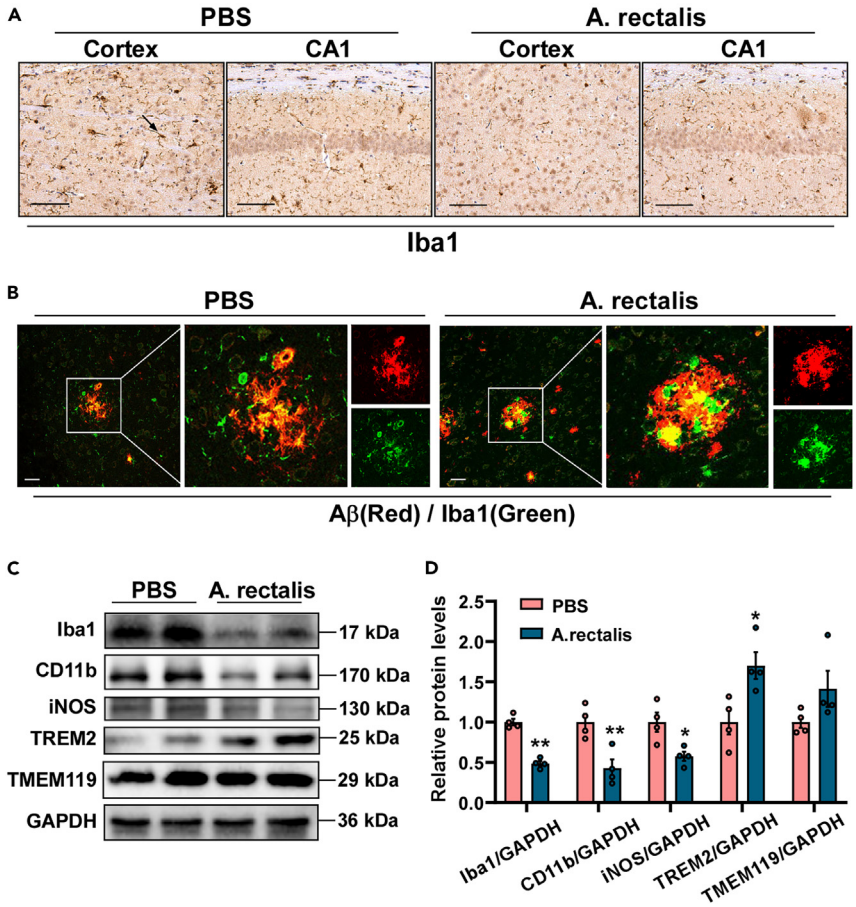

Figure 4. *A. rectalis* treatment suppressed microglia-mediated neuroinflammation in the APP/PS1 mice

(A) Immunohistochemistry analysis of Iba1 in the cortex and CA1 region of hippocampus. The black arrow represented polarized microglia. Magnification 200×; scale bar, 100 μm.

(B) Representative immunofluorescence images of Aβ (Red) and Iba1 (Green). Magnification 400×; scale bar, 50 μm.

(C) Representative western blot images of Iba1, CD11b, iNOS, TREM2, and TMEM119.

(D) Quantitative analysis of Iba1, CD11b, iNOS, TREM2, and TMEM119 expression. The ratio of Iba1/GAPDH, CD11b/GAPDH, iNOS/GAPDH, TREM2/GAPDH, and TMEM119/GAPDH in the PBS-treated group were used as the reference value. Data are shown as mean ± SEM. *p values* were determined by unpaired two-tailed t test (D, except for Tmem119) or Mann-Whitney test (D, Tmem119). *$p < 0.05$ vs. PBS-treated group; **$p < 0.01$ vs. PBS-treated group.

group ($p < 0.01$, Figures S2E and S2F). These results suggested that butyric acid could suppress inflammatory microglia activation of AD by regulating Akt/NF-κB pathway.

A. rectalis treatment regulated the Akt/NF-κB pathway and improved abnormal gut microbiota of APP/PS1 mice

To confirm whether *A. rectalis* regulated the AKT/NF-κB signaling pathway, we determined the levels of Akt-/NF-κB-pathway-related proteins in the APP/PS1 mice. The ratio of p-Akt/Akt in the *A. rectalis*-treated mice was increased significantly compared with that in the PBS-treated mice ($p < 0.01$, Figures 7A and 7B), whereas that the ratio of p-p65/p65 in the *A. rectalis*-treated mice was decreased significantly compared with that in the PBS-treated mice ($p < 0.05$, Figures 7A and 7B). These findings suggested that the potential mechanism of *A. rectalis*-regulated neuroinflammation of AD might be borne on Akt/NF-κB signal pathway.

To further confirm the role of *A. rectalis* on the regulation of gut microbiota in AD, we performed 16s rRNA sequencing of fecal samples in the APP/PS1 mice. As shown in Figures 7C and 7D, α-diversity, as measured by Shannon and Simpson indices, showed no significant difference between the *A. rectalis*-treated mice and PBS-treated mice. The Venn diagram in Figure 7E showed there were 625 and 579 specific ASVs in the PBS-treated group and the *A. rectalis*-treated group, respectively, and 153 ASVs were shared in two groups. In addition, PCoA analysis (Figure 7F) and composition diagram of the community (Figure 7G) separately showed that the structure and taxa of gut microbiota were distinguishable between the *A. rectalis*-treated mice and PBS-treated mice. Eventually, we determined the level of *A. rectalis* and observed a significant increase in the abundance of *A. rectalis* in the *A. rectalis*-treated mice compared to the PBS-treated mice ($p < 0.05$, Figure 7H),

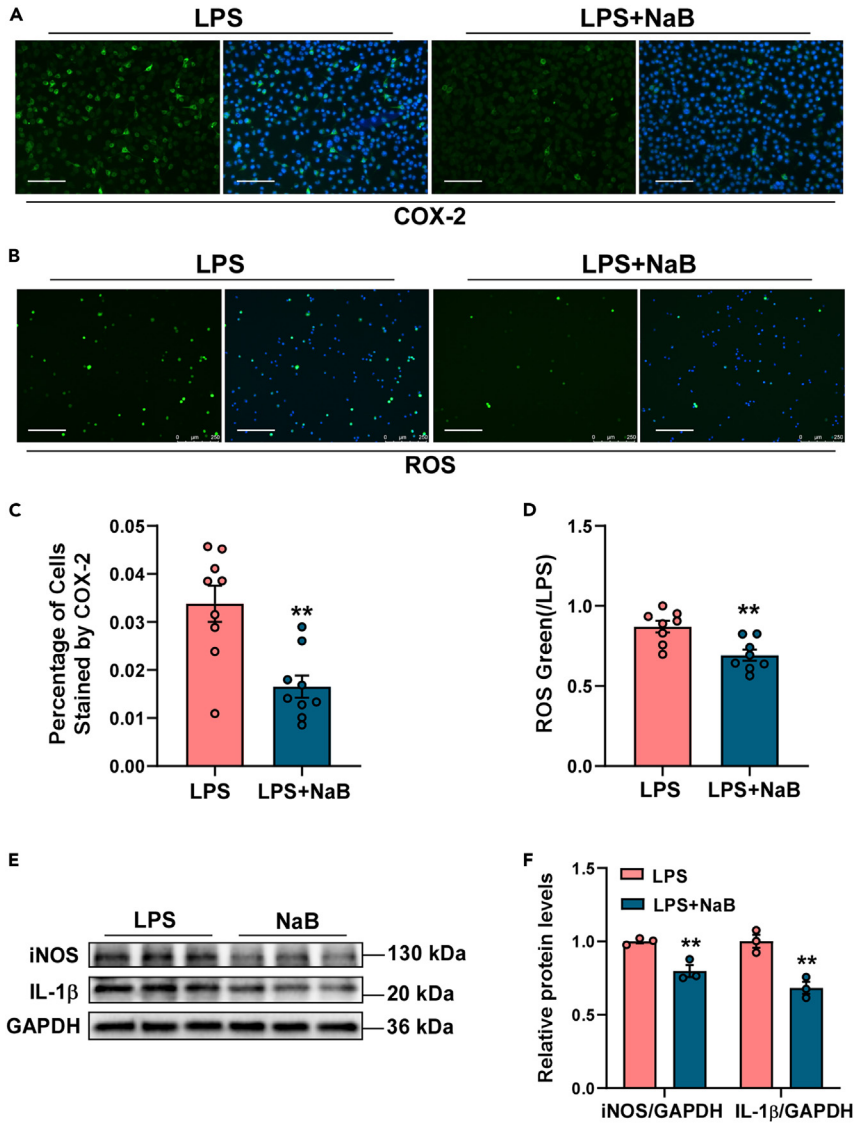

Figure 5. Butyric acid suppressed microglia-mediated neuroinflammation in LPS-induced BV2 cells

(A) Representative immunofluorescence images of COX-2. Magnification 200×; scale bar, 100 μm.

(B) Representative immunofluorescence images of ROS. Magnification 100×; scale bar, 250 μm.

(C) Quantitative analysis of COX-2.

(D) Quantitative analysis of ROS.

(E) Representative western blot images of iNOS and IL-1β.

(F) Quantitative analyses of iNOS and IL-1β expression. The ratios of iNOS/GAPDH and IL-1β/GAPDH in the LPS group were separately used as the reference value. Data are shown as mean ± SEM. *p* values were determined by unpaired two-tailed t test (C, D, and F). $^{**}p < 0.01$ vs. LPS group.

suggesting that *A. rectalis* could colonize in mice and exert biological effects. These results indicated that *A. rectalis* could regulate the abnormality of gut microbiota-gut-brain axis in AD.

DISCUSSION

Gut microbiota play a vital role in the regulation of neuroinflammation in AD.[6,18] However, the role of commensal bacteria from gut microbiota on microglia-mediated neuroinflammation in AD remains underexplored. In this study, we observed a markedly decreased abundance of *Agathobacter* in AD patients, and *Agathobacter* abundance was negatively correlated with cognitive impairment. *A. rectalis* supplementation could improve cognitive impairment and pathological damages and suppress microglial activation in the APP/PS1 mice. Most importantly, butyric acid, a metabolite of *A. rectalis*, could suppress microglial activation via regulating Akt/NF-κB pathway *in vitro*. We further revealed

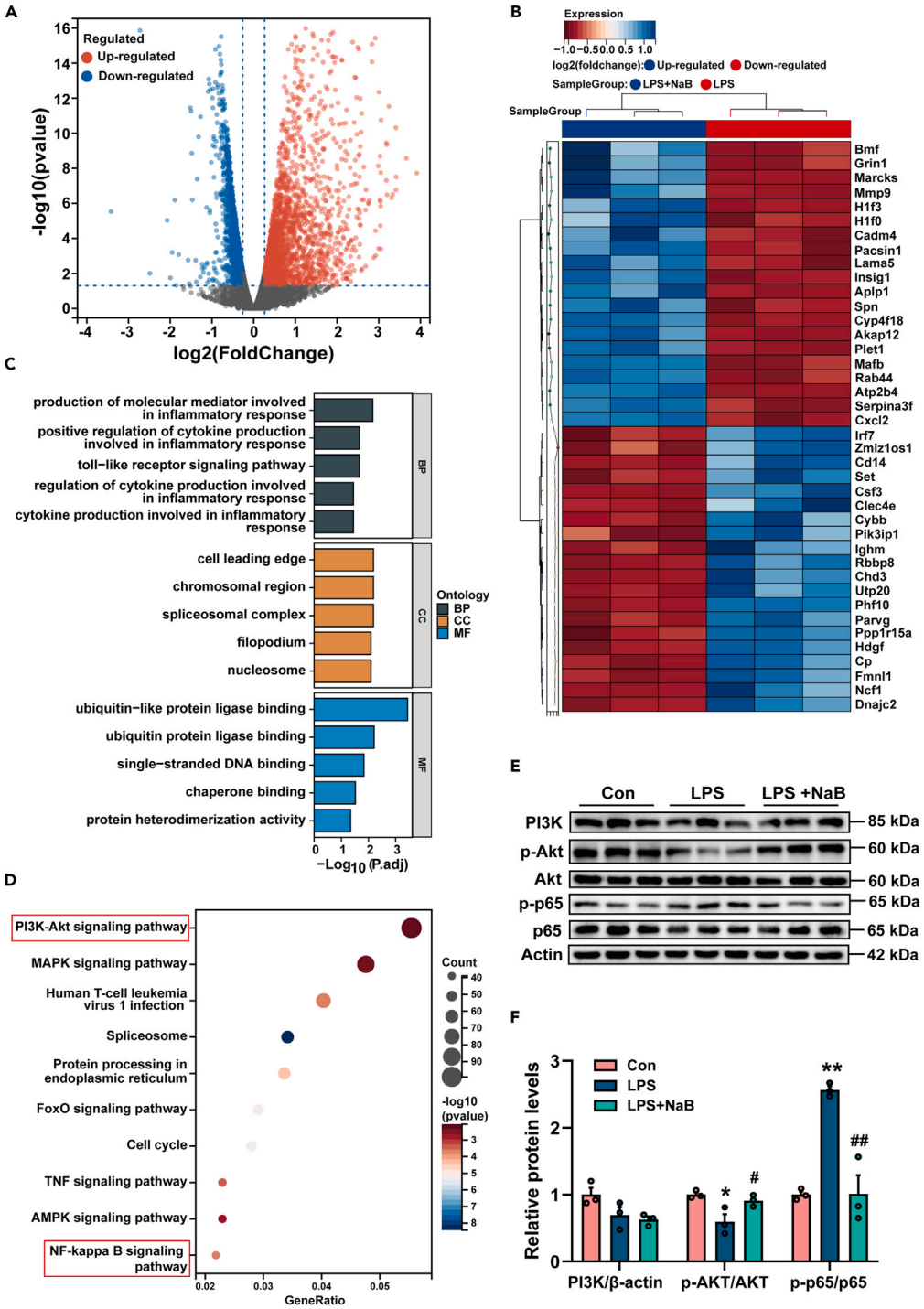

Figure 6. Butyric acid treatment suppressed microglia activation of AD via regulating Akt/NF-κB pathway

(A) Volcano plot showing the distribution of gene expression level differences between the LPS group and LPS + NaB group. *p*-adjusted <0.05 for FDR was screened as differentially expressed genes.

(B) Heatmap showing differentially expression genes between the LPS group and LPS + NaB group.

(C) GO analysis showing the biological functions of DEGs. The significant changes in inflammation-related pathways were found.

(D) KEGG pathway enrichment showing the PI3K-Akt and NF-κB pathways was significant enriched in DEGs between the LPS group and LPS + NaB group. *p*-adjusted <0.05 for FDR was considered statistically significant.

(E) Representative western blot images of Akt-/NF-κB pathway-related proteins, including PI3K, pAkt, Akt, p-p65, and p65.

Figure 6. *Continued*

(F) Quantitative analysis of Akt-/NF-κB-pathway-related proteins. The ratios of PI3K/Actin, pAkt/Akt, and p-p65/p65 in the Con group were separately used as the reference value. Data are shown as mean ± SEM. *p* values were determined by one-way ANOWA (F). **p* < 0.05 vs. Con group; ***p* < 0.01 vs. Con group; #*p* < 0.05 vs. LPS group; ##*p* < 0.01 vs. LPS group.

that *A. rectalis* treatment could regulate Akt/NF-κB pathway in the APP/PS1 mice. These findings suggested that *A. rectalis* might inhibit microglia-mediated neuroinflammation: involvement of the gut-brain axis and Akt/NF-κB pathway.

A. rectalis (formerly *Eubacterium rectale*), a butyric acid producing bacteria belonging to the *Lachnospiraceae* family, is considered a prevalent species of the human gut microbiota, with a beneficial effect on the host.[19,20] Our results revealed the abundance of *Agathobacter* in AD patients was deficient, and negatively correlated with MMSE and MOCA scores, indicating that *Agathobacter* might be a protective factor. Recent studies have reported that *Agathobacter* was a beneficial bacterium in the gastrointestinal tract, and the decreased abundance of *Agathobacter* was relevant to many neurological diseases, such as spinal cord injury,[21] postherpetic neuralgia,[22] and lacunar cerebral infarction.[23] Gut commensal *Agathobacter* might be involved in the neuroprotection of AD. This study evaluated the effects of *A. rectalis* administration on microglial activation and Alzheimer's pathology in APP/PS1 mice. Our results demonstrated that *A. rectalis* administration could reduce the Aβ accumulation and tau hyperphosphorylation of AD, inhibit microglial activation, and eventually improve cognitive impairment. Further research is required to clarify the related molecular mechanisms of *A. rectalis*-inhibited microglia-mediated neuroinflammation in AD.

Abnormal microglia polarization is a key pathogenesis mechanism of AD.[24] As primary immune cells of the brain, microglia contribute largely to the neuroinflammatory response and influence pathological process of AD.[25,26] Microglia, important executors of neuroinflammation in the brain, are regulated by gut microbiota.[11] Gut microbiota can participate in various stages of maturation and activation of microglia. Microglia of germ-free (GF) mice remain in an immature state, similar to those cleared by antibiotics, whereas the maturation or activation of microglia can be achieved by re-colonizing microbiota,[27,28] suggesting that gut microbiota can regulate microglia activation. The changes in gut microbiota directly alter their metabolites, which are the functional executors of the gut-brain axis. It is worth noting that *B. producta*, a butyrate-producing bacteria, exert beneficial effects by producing butyric acid. SCFA butyric acid is the main metabolite of human gut microbiota, which can enter the circulation from the intestine and then enter the brain.[29,30] In addition, we observed a significant reduction in butyric acid level in the AD group compared to the HC group and a positive association between the abundance of *Agathobacter* and butyric acid level, indicating that butyric acid might be the executor of *Agathobacter* in inhibiting microglial activation of AD. Then, we analyzed the effect of butyric acid on microglia activation *in vitro*. Our results demonstrated that butyric acid treatment significantly reduced the levels of COX-2, iNOS, and ROS in the LPS-induced BV2 microglia, suggesting that butyric acid could inhibit M1 microglial polarization. Our previous study revealed that SCFA acetate significantly decreased the CD11b level in the Aβ-stimulated BV2 microglia via regulating GPR41/NF-κB pathway, eventually inhibited microglial activation, and exerted anti-neuroinflammatory effects.[14] However, the possible mechanisms of butyric acid on microglia-mediated neuroinflammation of AD have yet to be elucidated. Therefore, this study provides further insights into the potential mechanisms of butyric acid effects. We proposed a more precise mechanism that may elucidate how *A. rectalis* inhibits microglial activation in AD. In this study, we performed RNA-seq analysis to explore the transcriptomic differences in AD cell models treated with butyric acid. Through the application of GO terms enrichment analysis, we were able to elucidate that the primary biological processes influenced by butyrate treatment were predominantly anti-inflammatory and immunomodulatory effects. Then, KEGG enrichment analysis found butyric acid suppressed microglia activation by regulating Akt/NF-κB pathway. Concurrently, we demonstrated that treatment with *A. rectalis* can modulate the Akt/NF-κB pathway in the APP/PS1 mice, thereby confirming the molecular mechanism through which *A. rectalis* inhibited microglial activation in AD. Akt/NF-κB pathway is recognized as one of the most critical signal transduction systems, underscoring its importance in this study. Akt signaling pathway is closely related to the development of AD and neuroinflammation.[31] Akt signaling pathway can regulate downstream-related proteins and exert important biological effects, including regulating microglial polarization.[32,33] Akt signaling pathway can participate in neuroinflammation by regulating inflammation-related cytokines. It was reported that Aβ aggregates could activate microglia via NF-κB pathways and promote the pro-inflammatory factors production, such as TNF-α, IL-1β, and IL-6, which might in turn exacerbate the disease. NF-κB is widely expressed in microglia and triggered neuroinflammatory responses.[34,35] Activation of the NF-κB signaling pathway upregulates downstream factors (including COX-2 and iNOS), leading to the excessive release of pro-inflammatory cytokines and heightened neuroinflammatory response.[14,36] Targeting Akt/NF-κB inflammation-related signaling pathways might inhibit neuroinflammation and then prevent disease progression. Thus, *A. rectalis*, noted for its butyrate production, plays a key role in mitigating neuroinflammation in AD, specifically through the regulation of Akt/NF-κB pathway, which would become the landmark reference to elucidate the causal relationship between specific gut microbiota and AD.

In conclusion, integrating the profiling of gut microbiota, metabolic features, and clinical features could provide a deep understanding of the specific bacteria and AD. Our findings suggested that *A. rectalis*-deficient and reduced fecal SCFA butyric acid level might contribute to neuroinflammation of AD. The present findings have important implications that *A. rectalis*-derived butyrate might be involved in the suppression of microglia-mediated neuroinflammation through regulating Akt/NF-κB pathway. Our study findings provided insights into causal relationship between gut microbiota and AD and suggested specific members from gut microbiota as promising therapeutic targets for combating AD.

Limitations of the study

Although our research delved into the experimental verification of *A. rectalis* functioning as a key role in mitigating neuroinflammation in AD, it should be acknowledged that *A. rectalis* can exhibit diverse functions, and there might be additional regulatory mechanisms yet to be explored. Future research should aim to uncover alternative mechanisms through which *A. rectalis* impacts gut microbiota and gut-brain axis.

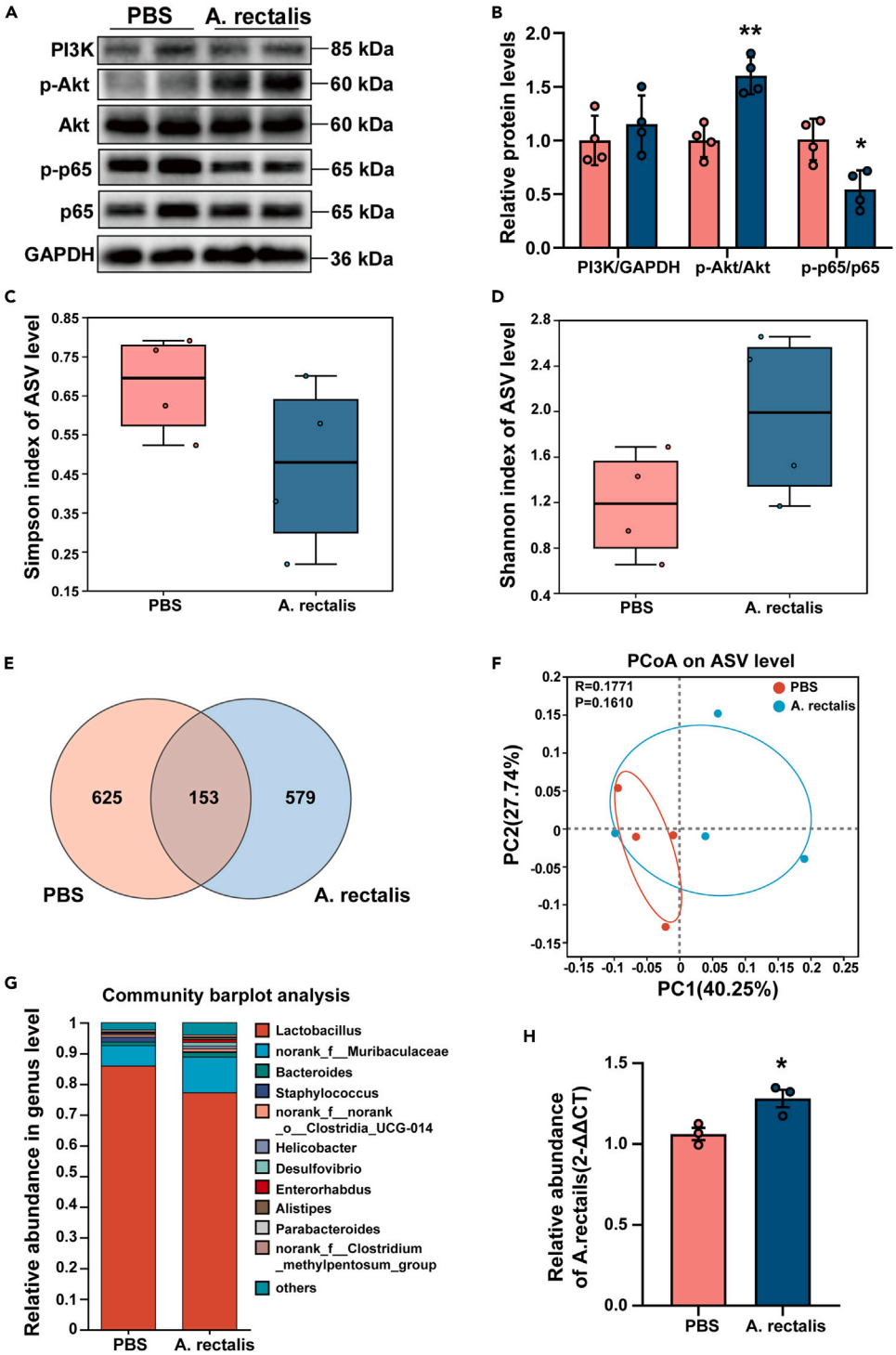

Figure 7. *A. rectalis* treatment regulated the Akt/NF-κB pathway and improved abnormal gut microbiota of APP/PS1 mice

(A) Representative western blot images of PI3K, Akt, p-Akt, p-65, and p-p65.

(B) Quantitative analysis of Akt-/NF-κB-pathway-related proteins. The ratios of PI3K/GAPDH, p-Akt/Akt and p-p65/p65 in the PBS-treated group were separately used as the reference value.

(C) Comparisons of Simpson index of gut microbiota α-diversity between two groups.

(D) Comparisons of Shannon index of gut microbiota α-diversity between two groups.

(E) Venn diagram illustrating the overlap of ASVs in gut microbiota.

Figure 7. *Continued*

(F) PCoA showing the differences of bacterial community between two groups.

(G) Stacked bar chart displaying the community structure composition and relative abundance of genus level.

(H) Comparisons of *A. rectalis* level between two groups. Data are shown as mean ± SEM (B and H) or medians and interquartile ranges (C and D). *p* values were determined by unpaired two-tailed t test (B and H) or Mann-Whitney test (C and D). *$p < 0.05$ vs. PBS-treated group; **$p < 0.01$ vs. PBS-treated group.

RESOURCE AVAILABILITY

Lead contact

Requests for resources and reagents should be directed to and will be fulfilled by the lead contact, Jiaming Liu (wzjiaming_liu@163.com).

Materials availability

This study did not generate new unique reagents.

Data and code availability

- The RNA-Seq raw data are available under the accession number SRA: PRJNA1159515. The raw data of 16s rRNA-Seq in mice is available under the accession number SRA: PRJNA1061810. The raw data of 16s rRNA-Seq in human is available under the accession number SRA: PRJNA1164845. Accession numbers are listed in the key resources table. Other data reported used during the current study are available from lead contact author on reasonable request.
- This paper does not report original code.
- Any additional information required to reanalyze the data reported in this work paper is available from the lead contact upon request.

ACKNOWLEDGMENTS

This study was funded by Major Program of Science and Technology Foundation of Wenzhou Municipality (No. ZY2022004). The graphic abstract was created using Figdraw (https://www.figdraw.com/#/).

AUTHOR CONTRIBUTIONS

The article was drafted by J.L. and J.S. The concept for this study's design was created by J.L. and J.S. The experiment was finished and the data were examined by X.L., L.Z., T.Y., and X.L. The data were processed and ideas were supplemented by H.X., Z.C., and Y.L. The data as well as the article were corrected by X.C. and W.Y. The final article was read and approved by all authors.

DECLARATION OF INTERESTS

The authors have declared no conflict of interest.

STAR★METHODS

Detailed methods are provided in the online version of this paper and include the following:

- KEY RESOURCES TABLE
- EXPERIMENTAL MODEL AND STUDY PARTICIPANT DETAILS
  - Animals
  - Human subjects
  - Cells
  - Bacteria
- METHOD DETAILS
  - 16s rRNA-sequencing in human and mice samples
  - Measurement of butyric acid content in human samples
  - Nesting behavior test
  - Object recognition test
  - Barnes maze test
  - Detection of *A. rectalis* in mice samples
  - Histopathology analysis in tissues
  - ROS detection
  - RNA-seq and data analysis
  - Immunofluorescence of proteins in cells
  - Real-time PCR
  - Western blot of proteins in tissues and cells
- QUANTIFICATION AND STATISTICAL ANALYSIS

SUPPLEMENTAL INFORMATION

Supplemental information can be found online at https://doi.org/10.1016/j.isci.2024.111116.

Received: May 1, 2024
Revised: August 15, 2024

Accepted: October 3, 2024
Published: October 5, 2024

REFERENCES

1. Kazmi, S.A., and Hsiao, E.Y. (2023). Extending genetic risk for Alzheimer's disease from host to holobiont. Cell *186*, 690–692. https://doi.org/10.1016/j.cell.2023.01.004.
2. Willyard, C. (2021). How gut microbes could drive brain disorders. Nature *590*, 22–25. https://doi.org/10.1038/d41586-021-00260-3.
3. Sorboni, S.G., Moghaddam, H.S., Jafarzadeh-Esfehani, R., and Soleimanpour, S. (2022). A Comprehensive Review on the Role of the Gut Microbiome in Human Neurological Disorders. Clin. Microbiol. Rev. *35*, e0033820. https://doi.org/10.1128/cmr.00338-20.
4. Seo, D.o., Boros, B.D., and Holtzman, D.M. (2019). The microbiome: A target for Alzheimer disease? Cell Res. *29*, 779–780. https://doi.org/10.1038/s41422-019-0227-7.
5. Wang, J., Gu, B.J., Masters, C.L., and Wang, Y.J. (2017). A systemic view of Alzheimer disease - insights from amyloid-β metabolism beyond the brain. Nat. Rev. Neurol. *13*, 612–623. https://doi.org/10.1038/nrneurol.2017.111.
6. Sun, J., Xu, J., Ling, Y., Wang, F., Gong, T., Yang, C., Ye, S., Ye, K., Wei, D., Song, Z., et al. (2019). Fecal microbiota transplantation alleviated Alzheimer's disease-like pathogenesis in APP/PS1 transgenic mice. Transl. Psychiatry *9*, 189. https://doi.org/10.1038/s41398-019-0525-3.
7. Sun, J., Zhang, Y., Kong, Y., Ye, T., Yu, Q., Kumaran Satyanarayanan, S., Su, K.P., and Liu, J. (2022). Microbiota-derived metabolite Indoles induced aryl hydrocarbon receptor activation and inhibited neuroinflammation in APP/PS1 mice. Brain Behav. Immun. *106*, 76–88. https://doi.org/10.1016/j.bbi.2022.08.003.
8. Liu, L., Tong, F., Li, H., Bin, Y., Ding, P., Peng, L., Liu, Z., and Dong, X. (2023). Maturation, Morphology, and Function: The Decisive Role of Intestinal Flora on Microglia: A Review. J. Integr. Neurosci. *22*, 70. https://doi.org/10.31083/j.jin2203070.
9. Lukens, J.R., and Eyo, U.B. (2022). Microglia and Neurodevelopmental Disorders. Annu. Rev. Neurosci. *45*, 425–445. https://doi.org/10.1146/annurev-neuro-110920-023056.
10. Cryan, J.F., O'Riordan, K.J., Cowan, C.S.M., Sandhu, K.V., Bastiaanssen, T.F.S., Boehme, M., Codagnone, M.G., Cussotto, S., Fulling, C., Golubeva, A.V., et al. (2019). The Microbiota-Gut-Brain Axis. Physiol. Rev. *99*, 1877–2013. https://doi.org/10.1152/physrev.00018.2018.
11. Lynch, C.M.K., Clarke, G., and Cryan, J.F. (2021). Powering up microbiome-microglia interactions. Cell Metabol. *33*, 2097–2099. https://doi.org/10.1016/j.cmet.2021.10.006.
12. Mossad, O., and Blank, T. (2021). Getting on in Old Age: How the Gut Microbiota Interferes With Brain Innate Immunity. Front. Cell. Neurosci. *15*, 698126. https://doi.org/10.3389/fncel.2021.698126.
13. Sun, J., Li, H., Jin, Y., Yu, J., Mao, S., Su, K.P., Ling, Z., and Liu, J. (2021). Probiotic Clostridium butyricum ameliorated motor deficits in a mouse model of Parkinson's disease via gut microbiota-GLP-1 pathway. Brain Behav. Immun. *91*, 703–715. https://doi.org/10.1016/j.bbi.2020.10.014.
14. Fann, D.Y.W., Lim, Y.A., Cheng, Y.L., Lok, K.Z., Chunduri, P., Baik, S.H., Drummond, G.R., Dheen, S.T., Sobey, C.G., Jo, D.G., et al. (2018). Evidence that NF-κB and MAPK Signaling Promotes NLRP Inflammasome Activation in Neurons Following Ischemic Stroke. Mol. Neurobiol. *55*, 1082–1096. https://doi.org/10.1007/s12035-017-0394-9.
15. Sun, J., Xu, J., Yang, B., Chen, K., Kong, Y., Fang, N., Gong, T., Wang, F., Ling, Z., and Liu, J. (2020). Effect of Clostridium butyricum against Microglia-Mediated Neuroinflammation in Alzheimer's Disease via Regulating Gut Microbiota and Metabolites Butyrate. Mol. Nutr. Food Res. *64*, e1900636. https://doi.org/10.1002/mnfr.201900636.
16. Erny, D., Dokalis, N., Mezö, C., Castoldi, A., Mossad, O., Staszewski, O., Frosch, M., Villa, M., Fuchs, V., Mayer, A., et al. (2021). Microbiota-derived acetate enables the metabolic fitness of the brain innate immune system during health and disease. Cell Metabol. *33*, 2260–2276.e7. https://doi.org/10.1016/j.cmet.2021.10.010.
17. Zhang, Y., Shen, Y., Liufu, N., Liu, L., Li, W., Shi, Z., Zheng, H., Mei, X., Chen, C.Y., Jiang, Z., et al. (2023). Transmission of Alzheimer's disease-associated microbiota dysbiosis and its impact on cognitive function: evidence from mice and patients. Mol. Psychiatr. *28*, 4421–4437. https://doi.org/10.1038/s41380-023-02216-7.
18. Liu, J., Ye, T., Zhang, Y., Zhang, R., Kong, Y., Zhang, Y., and Sun, J. (2021). Protective Effect of Ginkgolide B against Cognitive Impairment in Mice via Regulation of Gut Microbiota. J. Agric. Food Chem. *69*, 12230–12240. https://doi.org/10.1021/acs.jafc.1c05038.
19. Adrian, M.A., Ayati, B.P., and Mangalam, A.K. (2023). A mathematical model of Bacteroides thetaiotaomicron, Methanobrevibacter smithii, and Eubacterium rectale interactions in the human gut. Sci. Rep. *13*, 21192. https://doi.org/10.1038/s41598-023-48524-4.
20. Kogawa, M., Nishikawa, Y., Saeki, T., Yoda, T., Arikawa, K., Takeyama, H., and Hosokawa, M. (2023). Revealing within-species diversity in uncultured human gut bacteria with single-cell long-read sequencing. Front. Microbiol. *14*, 1133917. https://doi.org/10.3389/fmicb.2023.1133917.
21. Jing, Y., Yang, D., Bai, F., Wang, Q., Zhang, C., Yan, Y., Li, Z., Li, Y., Chen, Z., Li, J., and Yu, Y. (2023). Spinal cord injury-induced gut dysbiosis influences neurological recovery partly through short-chain fatty acids. NPJ Biofilms Microbiomes *9*, 99. https://doi.org/10.1038/s41522-023-00466-5.
22. Jiao, B., Cao, X., Zhang, C., Zhang, W., Yu, S., Zhang, M., and Zhang, X. (2023). Alterations of the gut microbiota in patients with postherpetic neuralgia. Amb. Express *13*, 108. https://doi.org/10.1186/s13568-023-01614-y.
23. Ma, J., Xie, H., Yuan, C., Shen, J., Chen, J., Chen, Q., Liu, J., Tong, Q., and Sun, J. (2024). The gut microbial signatures of patients with lacunar cerebral infarction. Nutr. Neurosci. *27*, 620–636. https://doi.org/10.1080/1028415x.2023.2242121.
24. Sun, N., Victor, M.B., Park, Y.P., Xiong, X., Scannail, A.N., Leary, N., Prosper, S., Viswanathan, S., Luna, X., Boix, C.A., et al. (2023). Human microglial state dynamics in Alzheimer's disease progression. Cell *186*, 4386–4403.e29. https://doi.org/10.1016/j.cell.2023.08.037.
25. McAlpine, C.S., Park, J., Griciuc, A., Kim, E., Choi, S.H., Iwamoto, Y., Kiss, M.G., Christie, K.A., Vinegoni, C., Poller, W.C., et al. (2021). Astrocytic interleukin-3 programs microglia and limits Alzheimer's disease. Nature *595*, 701–706. https://doi.org/10.1038/s41586-021-03734-6.
26. Bartels, T., De Schepper, S., and Hong, S. (2020). Microglia modulate neurodegeneration in Alzheimer's and Parkinson's diseases. Science *370*, 66–69. https://doi.org/10.1126/science.abb8587.
27. Matcovitch-Natan, O., Winter, D.R., Giladi, A., Vargas Aguilar, S., Spinrad, A., Sarrazin, S., Ben-Yehuda, H., David, E., Zelada González, F., Perrin, P., et al. (2016). Microglia development follows a stepwise program to regulate brain homeostasis. Science *353*, aad8670. https://doi.org/10.1126/science.aad8670.
28. Erny, D., Hrabě de Angelis, A.L., Jaitin, D., Wieghofer, P., Staszewski, O., David, E., Keren-Shaul, H., Mahlakoiv, T., Jakobshagen, K., Buch, T., et al. (2015). Host microbiota constantly control maturation and function of microglia in the CNS. Nat. Neurosci. *18*, 965–977. https://doi.org/10.1038/nn.4030.
29. Borre, Y.E., O'Keeffe, G.W., Clarke, G., Stanton, C., Dinan, T.G., and Cryan, J.F. (2014). Microbiota and neurodevelopmental windows: implications for brain disorders. Trends Mol. Med. *20*, 509–518. https://doi.org/10.1016/j.molmed.2014.05.002.
30. Kim, S.W., Hooker, J.M., Otto, N., Win, K., Muench, L., Shea, C., Carter, P., King, P., Reid, A.E., Volkow, N.D., and Fowler, J.S. (2013). Whole-body pharmacokinetics of HDAC inhibitor drugs, butyric acid, valproic acid and 4-phenylbutyric acid measured with carbon-11 labeled analogs by PET. Nucl. Med. Biol. *40*, 912–918. https://doi.org/10.1016/j.nucmedbio.2013.06.007.
31. Wang, S., Sudan, R., Peng, V., Zhou, Y., Du, S., Yuede, C.M., Lei, T., Hou, J., Cai, Z., Cella, M., et al. (2022). TREM2 drives microglia response to amyloid-β via SYK-dependent and -independent pathways. Cell *185*, 4153–4169.e19. https://doi.org/10.1016/j.cell.2022.09.033.
32. Zuo, H.J., Wang, P.X., Ren, X.Q., Shi, H.L., Shi, J.S., Guo, T., Wan, C., and Li, J.J. (2024). Gastrodin Regulates PI3K/AKT-Sirt3 Signaling Pathway and Proinflammatory Mediators in Activated Microglia. Mol. Neurobiol. *61*, 2728–2744. https://doi.org/10.1007/s12035-023-03743-8.

33. Bai, Y., Zhou, J., Zhu, H., Tao, Y., Wang, L., Yang, L., Wu, H., Huang, F., Shi, H., and Wu, X. (2023). Isoliquiritigenin inhibits microglia-mediated neuroinflammation in models of Parkinson's disease via JNK/AKT/NFκB signaling pathway. Phytother Res. *37*, 848–859. https://doi.org/10.1002/ptr.7665.

34. Matsui, T., Tasaki, M., Yoshioka, T., Motoki, Y., Tsuneoka, H., and Nojima, J. (2012). Temperature- and time-dependent changes in TLR2-activated microglial NF-κB activity and concentrations of inflammatory and anti-inflammatory factors. Intensive Care Med. *38*, 1392–1399. https://doi.org/10.1007/s00134-012-2591-3.

35. Wu, J., Han, Y., Xu, H., Sun, H., Wang, R., Ren, H., and Wang, G. (2023). Deficient chaperone-mediated autophagy facilitates LPS-induced microglial activation via regulation of the p300/NF-κB/NLRP3 pathway. Sci. Adv. *9*, eadi8343. https://doi.org/10.1126/sciadv.adi8343.

36. Liu, J., Li, H., Gong, T., Chen, W., Mao, S., Kong, Y., Yu, J., and Sun, J. (2020). Anti-neuroinflammatory Effect of Short-Chain Fatty Acid Acetate against Alzheimer's Disease via Upregulating GPR41 and Inhibiting ERK/JNK/NF-κB. J. Agric. Food Chem. *68*, 7152–7161. https://doi.org/10.1021/acs.jafc.0c02807.

37. Ye, T., Yuan, S., Kong, Y., Yang, H., Wei, H., Zhang, Y., Jin, H., Yu, Q., Liu, J., Chen, S., and Sun, J. (2022). Effect of probiotic fungi against cognitive impairment in mice via regulation of the fungal microbiota–gut–brain axis. J. Agric. Food Chem. *70*, 9026–9038. https://doi.org/10.1021/acs.jafc.2c03142.

STAR★METHODS

KEY RESOURCES TABLE

REAGENT or RESOURCE	SOURCE	IDENTIFIER
Antibodies		
Anti-Iba1	Abcam	Cat# ab153696; RRID: AB_2889406
Anti-Aβ1-42	Cell signaling Technology	Cat# 14974; RRID: AB_2798671
Anti-β-Amloid	Cell signaling Technology	Cat# 15126; RRID: AB_2798720
Anti-AT8	ABclonal	Cat# AP0894;
Anti-CD11b	Bioworld	Cat# BS6640;
Anti-TREM2	Bioworld	Cat# BZ17066;
Anti-TMEM119	Abclonal	Cat# A22118;
Anti-p-Tau(S202/T205)	Bioworld	Cat# BS1358; RRID: AB_1662409
Anti-PI3K	Abcam	Cat# ab302958;
Anti- p-Akt Ser473	Bioworld	Cat# BS4006;
Anti-p65	Bioworld	Cat# BS1560; RRID: AB_1662373
Anti-p-p65 Ser536	Bioworld	Cat# BS5088; RRID: AB_1661930
Anti-iNOS	Cell signaling Technology	Cat# D6B6S;
Anti-IL-1β	Bioworld	Cat# BS3506; RRID: AB_1661842
Anti-GAPDH	Bioworld	Cat# AP0063; RRID: AB_2651132
Anti-HRP beta Actin	Huabio	Cat# ET1702-67; RRID: AB_2890197
HRP-labeled Goat Anti-Rabbit IgG	Beyotime	Cat# A0208; RRID: AB_2892644
Bacterial and virus strains		
Agathobacter rectalis	ATCC	ATCC 33656
Biological samples		
Human feces samples	The second affiliated hospital of Wenzhou Medical university	N/A
Chemicals, peptides, and recombinant proteins		
Sodium butyrate	Sigma	156-54-7
Amyloid β Protein Fragment 1-42	Maclin	107761-42-2
Deposited data		
RNA-seq raw data	This paper	PRJNA1159515
Raw data of 16s rRNA-seq in mice	This paper	PRJNA1061810
Raw data of 16s rRNA-seq in human	This paper	PRJNA1164845
Critical commercial assays		
Reactive oxygen species Assay Kit	Nanjing Jiangcheng Bioengineering Insititute	E004-1-1
HiScript III RT SuperMix for qPCR (+gDNA wiper)	Vazyme	R323-01

(*Continued on next page*)

Continued

REAGENT or RESOURCE	SOURCE	IDENTIFIER
ChamQ Universal SYBR qPCR Master Mix kit	Vazyme	Q711-02
Experimental models: Cell lines		
BV2 cells	Shanghai Institutes for Biological Sciences	GNM45
Experimental models: Organisms/strains		
Mouse: APPswe/PSEN1dE9	Hangzhou Ziyuan Experimental Technology	N/A
Mouse: C57B/L6 N	Hangzhou Ziyuan Experimental Technology	N/A
Oligonucleotides		
Primer: P2ry12 F:ATGGATATGCCTGGTGTCAACA R:AGCAATGGGAAGAGAACCTGG	This paper	N/A
Primer: TMEM119 F:CCTACTCTGTGTCACTCCCG R:CACGTACTGCCGGAAGAAATC	This paper	N/A
Primer: KI67 F:CAAGGCGAGCCTCAAGAGATA R:TGTGCTGTTCTACATGCCCTG	This paper	N/A
Primer: TREM2 F:CTGGAACCGTCACCATCACTC R:CGAAACTCGATGACTCCTCGG	This paper	N/A
Primer: CD33 F:CCGCTGTTCTTGCTGTGTG R:AAGTGAGCTTAATGGAGGGGTA	This paper	N/A
Primer: APOE F:CTGACAGGATGCCTAGCCG R:CGCAGGTAATCCCAGAAGC	This paper	N/A
Primer: Ifi27l2a F:GCTTGTTGGGAACCCTGTTTG R:GGATGGCATTTGTTGATGTGGAG	This paper	N/A
Primer: IFI204 F:GACAACCAAGAGCAATACACCA R:ATCAGTTTGCCCAATCCAGAAT	This paper	N/A
Primer: CXCL10 F:CCAAGTGCTGCCGTCATTTTC R:GGCTCGCAGGGATGATTTCAA	This paper	N/A
Primer: iL1β F:GCAACTGTTCCTGAACTCAACT R:ATCTTTTGGGGTCCGTCAACT	This paper	N/A
Primer: TNF-α F:GACGTGGAACTGGCAGAAGAG R:TTGGTGGTTTGTGAGTGTGAG	This paper	N/A
Primer: iL6 F:TAGTCCTTCCTACCCCAATTTCC R:TTGGTCCTTAGCCACTCCTTC	This paper	N/A
Primer: A. rectalis F:CAAGGTGGTTGACGCTGTAG R: TCGGTGTCTGTCTCGAAGA	This paper	N/A
Software and algorithms		
Prism	9.5.0(730)	https://www.graphpad.com/features
ImageJ	1.52a	https://imagej.nih.gov/ij/

EXPERIMENTAL MODEL AND STUDY PARTICIPANT DETAILS

Animals

6-mouth old male adult APPswe/PSEN1dE9 transgenic mice (n = 12) and 6-mouth old male C57BL/6J mice (n = 6) were purchased from Hangzhou Ziyuan Experimental Technology Co, Ltd, Hangzhou, China. Animals were housed in rooms kept in a 12-hour light/12-hour dark cycle and allowed *ad libitum* to feed and water. APPswe/PSEN1dE9 transgenic mice (n = 6/group) were randomly divided into PBS-treated group and *A. rectalis*-treated group. After confirming the activity of *A. rectalis*, a PBS suspension of *A. rectalis* (1×10^9 CFU/mL) was daily gavaged to mice for 4 weeks, with PBS as controls. The behavioral tests were tested after stopping bacterial manipulations. The mice experiments were performed with the ethical approval by Animal Experiment Ethics Committee of Wenzhou Medical University (xmsq2022-0549).

Human subjects

The human microbiota study was approved by the Ethics Committee of the Second Affiliated Hospital of Wenzhou Medical University (2021199). A total of 21 AD patients (male: female: 7:14;age : 76.33 ± 8.48 years old) were recruited from the hospital between January 2022 and August 2023. All participants met the Alzheimer's Disease Diagnosis Guidelines in China (2020 Edition). 19 healthy controls (HC) (male: female: 9:10; age: 71.42 ± 7.00 years old) were also included in the study. Exclusion criteria for the study were as follows: (1) Imaging evidence of central nervous system-related cognitive dysfunction (e.g., stroke, hippocampal sclerosis, tumors); (2) Excessive alcohol consumption or use of medications for epilepsy, sleep disorders, or emotional conditions; (3) Untreated disorders that could affect cognitive evaluation (e.g., untreated thyroid disease, vitamin B12/folate deficiency); (4) Hearing or visual impairments or severe mental health conditions impacting the ability to complete assessments; (5) Use of probiotics, antibiotics, or specific diets within the past 3 months; (6) Severe health conditions (e.g., cancer, acute gastroenteritis, serious respiratory issues).The degree of cognitive impairment of subjects was assessed by the Mini-Mental State Examination (MMSE) and Montreal Cognitive Assessment (MoCA). Fresh fecal samples were collected from all participants within 1 week of admission and immediately analyzed for gut microbiota composition and butyric acid levels.

Cells

BV2 microglia cells were purchased from Shanghai Institutes for Biological Sciences (Shanghai, China). BV2 microglia cells were plated in DMEM supplemented with 10% (v/v) FBS (Sigma, Australia) and cultured at 37°C with 5% CO2 and a relative humidity of 95%. BV2 microglia cells were administrated with 1μg LPS (Sigma, USA) or 10μM aβ (Macklin, China) and 200 μM NaB (sodium butyrate, Sigma, USA) for 24 h.

Bacteria

Agathobacter strain (*A. rectalis*, ATCC, 33656) was cultured using Modified chopped meat medium ATCC medium 1490 supplementing 1 mg/L vitamin K1 and 5 mg/L heme (Shandong Tuopu Biol-engineering Co., Ltd, Shandong, China) under 37°C with anaerobic conditions (Bactron300 Anaerobic Chamber Glovebox, Shel Lab Inc.).

METHOD DETAILS

16s rRNA-sequencing in human and mice samples

Microbial DNA was extracted from stool samples using QIAamp DNA stool mini kit (Qiagen, Hilden, Germany). For 16S amplicon sequencing, the V3-V4 regions of bacterial 16S rRNA were amplified using the primers 338F (ACTCCTACGGGAGGCAGCAG) and 806R (GGACTACHVGGGTWTCTAAT) with thermocycler PCR system (GeneAmp 9700, ABI, USA), and the PCR products were purified using the AxyPrep DNA Gel Extraction Kit (Axygen Biosciences, Union City, CA, USA) and quantified using QuantiFluor™-ST (Promega, USA). Subsequently, sequencing libraries were generated, and the samples were sequenced on an Illumina MiSeq platform (Illumina, San Diego, USA). The high-throughput community sequences were clustered into the amplified sequence variant (ASV) with 100% similarity by DADA2 software. During the clustering process, individual sequences and chimeras were removed to filter out low-quality sequences or artifacts. The analysis was conducted on the community diversity, community composition and species differences of the gut microbiota. The α diversity was indicated using the Shannon and Simpson indices, and the β diversity was compared by principal coordinate analysis (PCoA) based on Bray-Curtis distances. The characteristics of gut microbiota were analyzed through Kruskal Wallis rank sum test and False-Discovery Rate (FDR) multiple correction test, and the threshold of Linear discriminant analysis (LDA) Effect Size (LEfSe) was 2.0.

Measurement of butyric acid content in human samples

Fecal samples were weighed to 20 mg, complemented with 800 μl water containing 0.5% phosphoric acid and 10 μg/mL internal standard 2-ethylbutyric acid, and the mixture was homogenized using High throughput tissue crusher Wonbio-96c (Shanghai wanbo biotechnology co., LTD) at a frequency of 50 Hz at 4° C for 6 min, ultrasound for 10 min, and centrifuged at 13, 000 rpm at 4°C for 15 min. The supernatant was extracted using N-butanol solvent containing 10 μg/mL internal standard 2-ethylbutyric acid, followed by ultrasonic for 10 min and centrifugation at 13, 000 rpm at 4°C for 15 min, and then, was transferred to sample vials for GC-MS analysis. GC-MS analysis was conducted on the Agilent 8890B gas chromatography coupled to an Agilent 7000D mass selective detector (Agilent Technologies Inc. CA, USA). The GC system was equipped with an HP-FFAP capillary column (30 m × 0.25 mm × 0.25 μm; Agilent J&W Scientific, Folsom, CA, USA) and high-purity helium was used as the carrier gas at 1.0 mL/min. The injection was performed in split mode with a volume of 1 μL and an injector temperature of

180°C, and the column temperature was programmed with an initial temperature of 80°C and final temperature of 220°C. The detector was operated using an inert electron impact (EI) ionization source and the scanning mode was selected ion monitoring. The ion fragment of target butyric acid was automatically identified and scored by MassHunter quantitative software (Agilent Technologies Co., Ltd., USA, No. V10.0.7707.0). The content of butyric acid was calculated through a standard curve.

Nesting behavior test

Nesting behavior test was carried out in clean cages, which contained 1 cm thick padding with 30 pieces of paper (5 cm × 5 cm) placed evenly on it. Each mouse was placed in a cage, the nesting state was observed after 12 h and recorded through photograph as our previously described.[37]

Object recognition test

Object recognition test was conducted in an open cardboard box (40 cm × 40 cm × 40 cm). In the training phase, each mouse was positioned into the box with two identical rectangular wooden blocks and allowed to explore for 5 min. After 24 h, one of the rectangular wooden blocks was replaced by a cylindrical wooden block, and the time of mice spent on new object (TN) and familiar object (TF) was recorded. The box and blocks were cleaned with alcohol after each test to ensure that there were no residual odors or traces interfering. The discriminant index (DI) was calculated as follows: DI = (TN – TF) / (TN + TF) × 100%.

Barnes maze test

The Barnes maze was operated on a circular workbench with a diameter of 100 cm, surrounded by 20 equally spaced escape holes, and a black escape box was connected to one of the holes. The Barnes maze lasted for 6 consecutive days with three stages: adaptation (day 1st), training (day 2nd to 5th) and testing (day 6th). In the adaptation, each mouse was gently guided into the target hole and adapted to the escape box for 4 min. During the training phase, each mouse was placed in a plastic cylinder (20 cm in diameter, 27 cm in height) at the center of the maze and restricted to activity for 5 s. Subsequently, the cylinder was removed, each mouse was allowed to find the escape box for 3 min, and the time the four limbs of mouse entering the target box was recorded as latency. In the testing, the circular workbench was divided into four quadrants, and the escape box was in the center of a target quadrant. Then the target box was removed, and the time spent in the target quadrant of mouse was recorded.

Detection of *A. rectalis* in mice samples

Quantitative polymerase chain reaction (qPCR) was used to determine the abundance of *A. rectalis* in fecal samples. The genomic DNA (gDNA) of the fecal microbiota was extracted using an alkaline lysis method. The primers used for *A. rectalis* were provided in key resources table. For total bacteria, we utilized the 16s rRNA primers, then, real-time PCR was conducted on the gDNA of each sample. The abundance of bacteria was computed in relative units, normalized to the total bacteria present in the sample. ΔCt value was the difference between the Ct value of *A. rectalis* and the Ct value of total bacteria. The relative abundance was then determined using the 2-ΔΔCt method.

Histopathology analysis in tissues

The brain samples of mice were quickly dissected and fixed with 4 % paraformaldehyde for 24 h, put in a gradient concentration of alcohol for dehydration, and transparent with xylene. Afterwards, the samples were embedded in wax blocks and cut into 5 μm paraffin sections. The sections were respectively stained with Nissl staining, Immunohistochemistry and Immunofluorescence analysis. In Nissl staining, the slices were baked in a 65°C incubator for 2 h, dewaxed with xylene and rehydrated with gradient concentration of alcohol. Then, the slices were stained with Nissl Staining Solution (C0117, Beyotime, Shanghai, China) for 30 min, washed with distilled water, dehydrated with gradient alcohol and transparent in xylene. The slices were finally covered by neutral gum and observed the Nissl bodies under microscope and recorded. In Immunohistochemistry, the slices were subjected to antigen repair in citric buffer for 10 min, incubated with 3 % peroxidase at room temperature for 15 min, sealed with 5 % BSA at room temperature for 30 min, and incubated overnight with Iba1 primary antibody (1: 200, ab153696, Abcam, Cambridge, UK) at 4°C, then the slices were reheated at 37°C for 3 min and incubated with the second antibody at 37°C for 30 min after washing in PBA for 15 min. Subsequently, the slices were stained with diaminobenzidine (DAB), labeled the nucleus with hematoxylin for 1 min and sealed after alcohol dehydration and xylene transparency. The positive expression of brown particles was observed under the microscope and photographed. In Immunofluorescence, the slices were incubated with the primary antibody at 4°C overnight, including $A\beta_{1\text{-}42}$ (1: 200, #14974, Cell signaling Technology, Massachusetts, USA), p-Tau (1: 200, AP0894, ABclonal, Wuhan, China) and Iba1 (1: 200, ab153696, Abcam, Cambridge, UK),β-Amloid (1: 200, #15126, Cell signaling Technology, Massachusetts, USA), then, the slices were rinsed with PBS for 15 min and incubated with fluorescent secondary antibody at 37°C for 30 min. The nucleus of slices was further stained with DAPI, and the slices were blocked with anti-fluorescence quenching agent and observed under a fluorescence microscope.

ROS detection

The intracellular ROS production was determined using Reactive oxygen species Assay Kit (E004-1-1, Jiancheng, Nanjing, China). The LPS-induced BV2 microglia cells were incubated with 2,7-Dichlorofuorescin Diacetate (DCFH-DA), a sensitive ROS probe (1: 1000) at 37°C for 20 min, stained the nucleus with hoechst. The fluorescence intensity of DCFH-DA-stained cells was detected using fluorescence microscope.

RNA-seq and data analysis

Total RNA of the LPS-induced BV2 cells was extracted using TRIzol® Reagent according to the manufacturer's manual (Invitrogen) and the concentration, purity and integrity of total RNA were determined. mRNA separation, mRNA fragment, reverse transcription, cDNA library construction and Illumina sequencing were performed at Shanghai Majorbio Bio-pharm Biotechnology Co., Ltd. (Shanghai, China). To ensure the accuracy of subsequent bioinformatics analysis, the raw sequencing data was filtered using fastp (https://github.com/OpenGene/fastp), and then, the obtained high-quality clean data was assembled using Trinity (https://github.com/trinityrnaseq/trinityrnaseq/wiki). Initial assembly sequence was optimized and filtered using TransRate (http://hibberdlab.com/transrate/) and reassessed using BUSCO (Benchmarking Universal Single-Copy Orthologs, http://busco.ezlab.org). To identify the differentially expressed genes (DEGs), analysis of sample expression differences was performed using the edgeR (http://www.bioconductor.org/packages/2.12/bioc/html/edgeR.html) and the genes with P value < 0.05 and $|\log2FC| \geq 1.2$ were considered as DEGs. Subsequently, GO (Gene Ontology, http://www.geneontology.org/) and KEGG (Kyoto Encyclopedia of Genes and Genomes, http://www.genome.jp/kegg/) were used to classify and analyze functional and pathway changes and FDR <0.05 was considered significant for enrichment.

Immunofluorescence of proteins in cells

After the incubation with NaB for 24 h, BV2 microglia cells were fixed by 4 % paraformaldehyde, permeabilized with 0.3 % Triton for 15 min, and sealed with 5 % BSA for 1 h. Then, the slices were incubated with the primary antibody COX2 (1: 200, AF7003, Affinity, Jiangsu, China) and then incubated with fluorescent secondary antibody. The nucleus of slices was further stained with DAPI and were blocked with anti-fluorescence quenching agent and observed under a fluorescence microscope.

Real-time PCR

Quantitative real-time polymerase chain reaction (qRT-PCR) was conducted with the ChamQ Universal SYBR qPCR Master Mix kit (Vazyme, China) following established protocols. The fold expression relative to the reference gene was determined using the $2^{-\Delta\Delta Ct}$ comparative method. Primer sequences are provided in key resources table.

Western blot of proteins in tissues and cells

The brain tissues of mice and BV2 microglia cells were obtained and homogenized by RIPA lysis buffer (P0013B, Beyotime, Shanghai, China). The total protein concentration was determined by BCA Protein assay kit (P0010S, Beyotime, Shanghai, China). The same amount of protein samples was loaded in 10 % SDS-PAGE gel for electrophoresis and transferred to PVDF membrane. The membrane was sealed in 5 % BSA at room temperature for 1 h and washed with PBS. Then the sealed membrane was incubated overnight with p-p65 (Ser536; 1: 1000, BS5088, Bioworld, Minnesota, USA), p65 (1: 1000, BS1560, Bioworld, Minnesota, USA), iNOS (1: 500, D6B6S, Cell signaling Technology, Massachusetts, USA), Iba1 (1: 1000, ab153696, Abcam, Cambridge, UK), CD11b(1: 1000, BS6640, Bioworld, Minnesota, USA), Trem2 (1: 1000, BZ17066, Bioworld, Minnesota, USA), Tmem119 (1: 1000, A22118, Abclonal, Wuhan, China), $A\beta_{1\text{-}42}$ (1: 1000, #14974, Cell signaling Technology, Massachusetts, USA), p-Tau (Ser202/Thr205; 1: 1000, AP0894, ABclonal, Wuhan, China), Tau (1: 1000, BS1358, Bioworld, Minnesota, USA), PI3K (1: 1000, ab302958, Abcam, Cambridge, UK), p-Akt (Ser473; 1:1000, BS4006, Bioworld, Minnesota, USA), Akt (1: 1000, BS1810, Bioworld, Minnesota, USA), IL-1β (1: 1000, BS3506, Bioworld, Minnesota, USA) and GAPDH (1: 1000, AP0063, Bioworld, Minnesota, USA) at 4°C overnight. The bands taken from the primary antibody were washed with PBS for three times and placed in the second antibody containing horseradish peroxidase (HRP) label (1: 2000, Beyotime, Shanghai, China) and the grey values of images were recorded, and the results were analyzed. GADPH was used as the loading control.

QUANTIFICATION AND STATISTICAL ANALYSIS

All statistical data were analyzed by SPSS 25.0 software and plotted with GraphPad Prism 8.0 software, which was displayed as mean ± standard error (SEM) or medians and interquartile ranges. Significant difference of normally distributed variables was determined by the t-test or one-way ANOVA tests. Non-normal distributed data were compared by the Mann-Whitney test. The correlation analysis was performed by Spearman correlation analysis. $P < 0.05$ represented a significant difference.